

System for the automated photothermal treatment of cutaneous vascular lesions

Dan E. Andersen

Lumenis, Inc.
2400 Condensa Street
Santa Clara, California 95051
E-mail: dandersen@lumenis.com

Marek A. Niczyporuk

719 Torrey Court
Palo Alto, California 94303

Michael W. Wiltberger

David G. Angeley*

Lumenis, Inc.
2400 Condensa Street
Santa Clara, California 95051

Abstract. It is well known that the use of tightly focused continuous wave lasers can be an effective treatment of common telangiectasia. In general, the technique requires the skills of a highly dexterous surgeon using the aid of optical magnification. Due to the nature of this approach, it has proven to be largely impractical. To overcome this, we have developed an automated system that alleviates the strain on the user associated with the manual tracing method. The device makes use of high contrast illumination, simple monochromatic imaging, and machine vision to determine the location of blood vessels in the area of interest. The vessel coordinates are then used as input to a two-dimensional laser scanner via a near real-time feedback loop to target, track, and treat. Such mechanization should result in increased overall treatment success, and decreased patient morbidity. Additionally, this approach enables the use of laser systems that are considerably smaller than those currently used, and consequently the potential for significant cost savings. Here we present an overview of a proof-of-principle system, and results using examples involving *in vivo* imaging of human skin. © 2004 Society of Photo-Optical Instrumentation Engineers. [DOI: 10.1117/1.1644117]

Keywords: robotics; machine vision; real-time imaging; lasers in medicine.

Paper 014009 received Apr. 1, 2003; revised manuscript received Jun. 17, 2003; accepted for publication Jun. 19, 2003.

1 Introduction

Current photonic-based approaches to the treatment of cutaneous vascular lesions generally require the delivery of high energy pulses with spot sizes that are large compared to the size of the targeted vessels.^{1,2} While the large spot size does mitigate losses due to light scattering, and potentially allows for a number of vessels to be treated simultaneously, it also requires the use of a large device and unnecessarily exposes adjacent tissue to collateral damage. Alternatively, it is possible to use a smaller, relatively low-power continuous wave (cw) laser that is tightly focused to a spot size approaching that of the targeted vessels themselves.³ This beam can then be swept along the vessel, thereby causing coagulation. Treatment performed in this manner can be extremely effective, but when operated manually it can be tedious, difficult, and time consuming.^{4,5} To ameliorate these problems and allow for a commercially viable device, we have developed a relatively simple, low-cost, proof-of-principle system to automatically identify and treat vascular lesions on skin. The system makes use of inexpensive components, such as a low-power laser source, a standard Intel Pentium II PC, and an integrated handpiece containing a monochrome video camera, illumination by light-emitting diodes, and a galvanometer-based scanner. An elegant multispectral imaging approach to solving this problem has also been reported.^{6–9} Our approach differs from theirs by virtue of our initial design constraints. We placed particular emphasis on the cost of goods, clinical robustness, ergonomics, and manufacturability of the system. As a result

of this, our device embodies different concepts with regard to illumination, image capture, vessel detection, beam delivery and laser scanning than theirs. The details of these aspects are presented in this paper.

2 System Design

2.1 Illumination, Imaging, and Acquisition

The tissue is illuminated using a number of light-emitting diodes (LEDs) (LED, Agilent, HLMP-BL16). This LED was chosen because it is sufficiently bright, is of low cost, and has high reliability. A peak emitting wavelength of 586 nm has been selected because of its avid absorption by both hemoglobin (HbO₂) and deoxy-hemoglobin (Hb) while still being reasonably well transmitted by the pigmented epidermis when compared to green light, as shown in Fig. 1. This provides for high-contrast images of both veins and arteries. Green light illumination proved to be less worthwhile, presumably due to its increased absorption in melanin.

In the system, a total of 16 LEDs are arranged in a circular or ring geometry. The primary direction of the emitted light is aimed towards the center of the camera's field of view at the tissue plane. The ring is placed near the camera such that a 20×20 mm zone at the tissue is uniformly illuminated. The LEDs are pulsed to provide momentarily higher brightness than their typically rated output. This is accomplished using a small rail-to-rail operational amplifier (National Semiconductor, LMC6484) to switch a MOSFET (Vishay, VN10KM) that connects the LEDs (and a set of current-limiting resistors)

*Current affiliation: General Dynamics Advanced Information Systems, 1115 Fifth Street SW, Charlottesville, VA 22902.

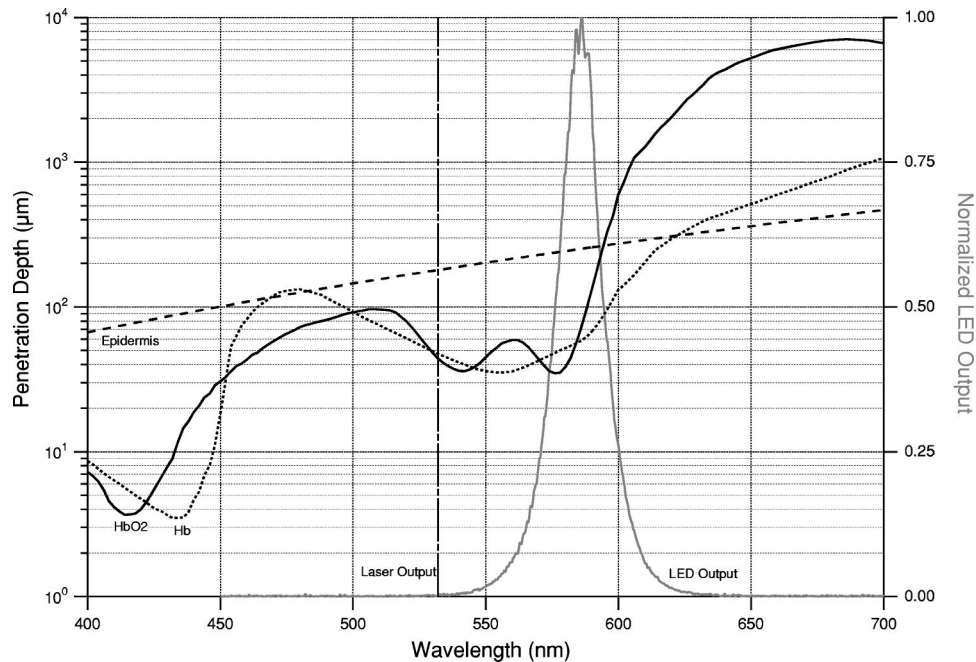


Fig. 1 Penetration depth ($\equiv \mu_a^{-1}$) versus wavelength for the predominant absorbers in skin. Blood absorption data courtesy of Peter Dwyer, Massachusetts General Hospital. The epidermal spectrum is modeled by assuming a 10% volume fraction, v_f , of melanosomes, such that $\mu_{a, \text{epidermis}} = v_f \mu_{a, \text{melanosome}}$. Melanosome absorption model courtesy of The Oregon Medical Laser Center, <http://omlc.ogi.edu/spectra/melanin/index.html>

across the PC's +5 V power supply. The command signal is synchronized with the camera's frame rate, and sent from the CPU (Micron PC, 550 MHz Pentium II) via a multifunction IO board (MIO, National Instruments, PCI-MIO-16E-4) that is connected to the CPU's PCI bus. See Fig. 2 for a system schematic.

Specular reflections are reduced by employing a ring-shaped linear polarizer (POL, Edmund Industrial Optics, 45668) near the light source and a crossed polarizer covering the entrance to the camera's aperture (ANA, Edmund Industrial Optics, 45668). At near-normal incidence, this crossed polarizer/analyzer configuration has an average extinction of 99.5% across the illumination band. This effectively eliminates spurious results generated by specular reflection from lines or wrinkles on the skin's surface, thus allowing for increased discrimination.^{10,11} As is standard clinical practice, the area to be treated is shaved prior to treatment in order to avoid unwanted absorption of the treatment beam by exposed hair follicles, which endangers the epidermis. This also eliminates the possibility of hair being mistaken for vessels by the image processing scheme.

The camera is a standard $\frac{1}{2}$ in. format RS-170 analog charge-coupled device (CCD) (CCD, WATEC, 902C) containing 768×494 pixels. The camera's signal-to-noise ratio of 48 dB matches well with the bit depth of the single-channel 8-bit image capture board (IMAQ, National Instruments, PCI-1409). A 12.5 mm focal length Computer lens [CBC (America) Corp., Torrance, CA] (L5 in Fig. 2) is used to image the tissue plane onto the CCD array. The proper magnification is achieved by employing the appropriate stand-off (7 cm from the lens' front flange) of the lens from the tissue plane. Measurements of the system's modulation transfer

function (object plane to detector) using a positive USAF 1951 test pattern demonstrate a value of 0.5 at a spatial frequency of 11 line pairs per millimeter at the tissue plane, indicating the ability to discern $90 \mu\text{m}$ features. Given the constraints of space and size, an image area consisting of the central 320×320 pixels on the CCD is set to cover a 20×20 mm tissue zone. The IMAQ board allows for the acquisition of partial images in a programmable region of interest, which has proven to be faster than cropping the image in software. LABVIEW software (National Instruments, version 5.1), running under Windows 2000, is used to coordinate the image data collection, laser control, and scanner positioning. It is also used to provide a graphical user interface that displays "live" video, including highlighting of the detected vessels (see Fig. 3). Highlighting is accomplished by rapidly scanning a 650 nm aiming laser beam along the detected vessels. This is done by inserting unprocessed images every fifth frame in "ready" mode so that the highlighted vessels appear to blink at 2 Hz in the displayed video image. The user is included in the safety loop by virtue of the fact that their consent must be given as a result of examining this display before treatment is initiated.

2.2 Vessel Detection

We employ directional matched filters for vessel enhancement.¹²⁻¹⁴ In this approach, vessels are considered to be barlike piecewise linear structures. For any given direction and width, vessels are enhanced using bar-shaped convolution masks composed of a central positive area to amplify the vessel's shape and surrounded by a negative neighborhood to suppress the vessel's background (Fig. 4). This basic approach has been shown to work in retinal images by employing a

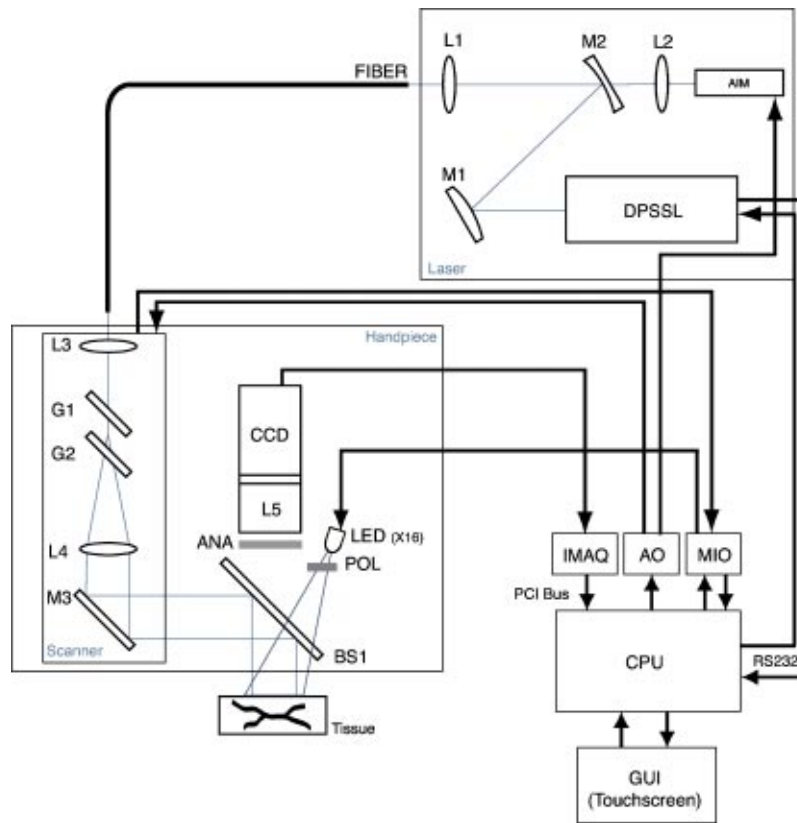


Fig. 2 System schematic.

cascade of such “thick” kernels with near-Gaussian profiles.¹² These Gaussian edge detectors are known to provide optimal edge localization and signal-to-noise response.^{15,16} However, the principal disadvantage of “thick” kernels is their extensive computational burden. An algorithm utilizing a computationally efficient set of directional matched filters that are sensitive to blood vessels of different orientations and thicknesses without sacrificing the desirable localization and signal-to-noise properties of Gaussian cylindrical convolution masks has been demonstrated. It was able to achieve a maximum bandwidth of only 13 Hz when running on a 300 MHz, DEC Alpha workstation.¹³ The value of added classification

constraints to increase the sensitivity of basic directional matched filters has also been reported; however, this comes at the cost of increased algorithmic complexity and computation time.¹⁴

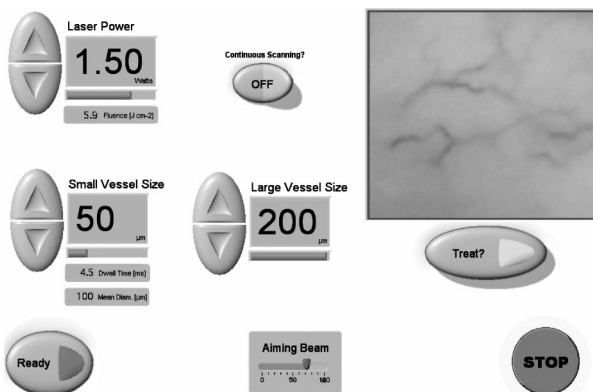


Fig. 3 Touchscreen GUI.

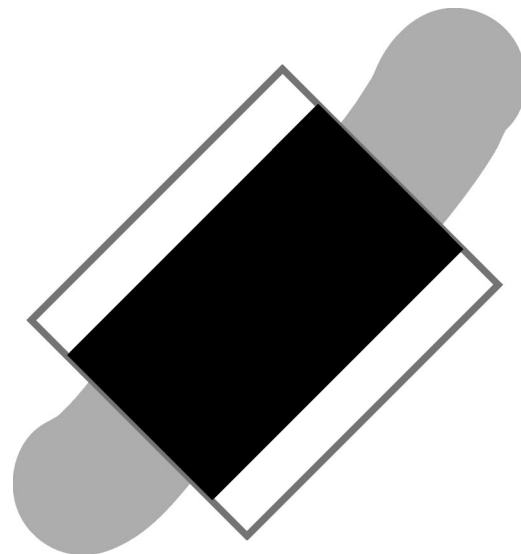


Fig. 4 Directional matched filters (“thick kernels”). By considering vessels to be barlike piecewise linear structures, vessels are enhanced using bar-shaped convolution masks composed of a central positive area to amplify the vessel’s shape, and surrounded by a negative neighborhood to suppress the vessel’s background.

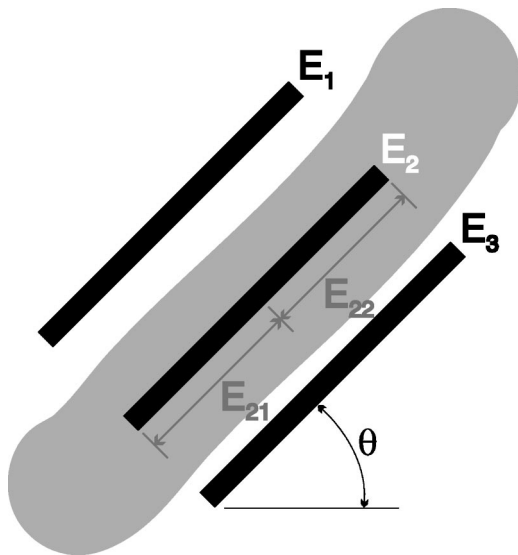


Fig. 5 Matched filter template with three edges, E_1 , E_2 , and E_3 , sampled along orientation angle θ . The central edge, E_2 , is divided into two half-segments, E_{21} and E_{22} . A cascade of such multidirectional and multiresolution filters is integrated, resulting in an enhanced image that best matches the vessel's geometry and contains the optimal response to both filter size and orientation.

For a handheld device we must accommodate normal resting tremor, which has been shown to have a dominant frequency component of 3.4 Hz with displacements that are on the order of our treatment beam's spot diameter.¹⁷ Our application, therefore, requires an overall bandwidth of ≥ 6.8 Hz to adequately track this motion. This puts a lower limit on our image processing speed that is "near real-time" as it is just below the frame rate limit that gives a human observer the illusion of continuity of motion. Our scheme also must be fully automated and self-optimizing since user input cannot be expected once treatment has begun. Furthermore, it must provide reproducible and accurate results in the presence of the ubiquitous noise and ambiguity in biological images. To satisfy these criteria, we have developed an algorithm that employs directional matched filters with added classification constraints. It provides a high degree of quality and sensitivity and operates at 10 Hz on a 550 MHz Pentium II PC. The cornerstone of this scheme is the assumption that vessels can be treated as barlike piecewise linear structures. The details of our algorithm and its development are to be given elsewhere.¹⁸ Alternative methods, such as morphological filters, probabilistic relaxation, and parallel gradient tracking have been shown to often work poorly on images with low contrast between blood vessels and their background, and do not always provide a continuous map of a blood vessel network.¹⁹

Our "thin" kernel is made up of three components, the U , A , and E operators, as shown in Fig. 5. The U operator emulates a cylindrical gaussian matched filter:

$$U = \pm(2E_2 - E_1 - E_3). \quad (1)$$

To improve the signal-to-noise ratio of U , images are first convolved with a low-pass Gaussian smoothing filter whose kernel size is smaller than smallest expected vessel diameter.

The E operator measures the nonuniformity of the vessel's background. This allows us to adjust the composite filter's response to simple steps and edges that are not entirely suppressed by the U operator alone:

$$E = -|E_1 - E_3|. \quad (2)$$

The A operator measures the intensity variations along a vessel. This attenuates the composite filter's response in the presence of nonuniformity along a vessel's ridge much like the well-known Duda Road operator,^{20,14}

$$A = -|E_{21} - E_{22}|. \quad (3)$$

The kernel's composite response V is calculated as follows:

$$V = U + eE + aA. \quad (4)$$

The weighting factors e and a may theoretically take on values between 0 and 1, but in practice are no larger than 0.5. Higher weights tend to suppress vessels in the presence of a highly nonuniform background or when there is considerable nonuniformity along the vessel itself, such as might be seen when a vessel winds through the skin.

In order to tackle the problem of vessel orientation, an array of filters, $V(\theta, S)$, is constructed at six different rotations ($\theta = 0^\circ, 27^\circ, 63^\circ, 90^\circ, 117^\circ, 153^\circ$) and at three different image scales ($S = 2d_{v,\min}, 2d_{v,\text{avg}}, 2d_{v,\max}$). The rotational values are chosen to be integer pixel steps in order to be quick and easy to compute. The filter scales are chosen corresponding to the expected range of vessel sizes ($d_{v,\min}, d_{v,\max}$) input by the user. At each image pixel, the optimal filter response, V_{opt} , is defined as the maximum response obtained over the range of computed orientations and scales:

$$V_{\text{opt}} = \max[V(\theta, S)]. \quad (5)$$

The vessel-enhanced image $V_{\text{opt}}(x, y)$ is then thresholded by a connectivity-based thresholding with hysteresis algorithm.^{15,16,13} Finally, morphological processing skeletonizes the isolated vessels to provide vector coordinates of the vessel's center lines for scanning.²¹⁻²³

Figures 6 and 7 show the results of our vessel detection algorithm on images of *in vivo* human skin containing a variety of vessel sizes.

2.3 Beam Delivery and Scanning

These skeletonized vessel maps are used to direct the application of the treatment laser by the scanner. A 2 W 532 nm diode-pumped solid state laser (DPSSL, Melles Griot, 58-GS-301) is used for treatment (see Fig. 2). The output of DPSSL is controlled via RS232. This laser has a measured power-dependent $M^2 = 3.2 \pm 0.2$, and a minimum waist diameter of 0.32 mm at the output coupler. At the output of the laser head, the beam is expanded and roughly collimated into a 3 mm diameter beam using a pair of reflecting spherical mirrors in a Galilean-like telescope configuration (M1 and M2, Absolute Coating, Custom). The angle of incidence at these two mirrors has been minimized to reduce astigmatism. The collimated beam is coupled into a 50 μm diameter, 0.12 numerical aperture (NA) optical fiber (Lumenis, LLA 11479) using a 12.5 mm focal length achromatic doublet (L1, Edmund Industrial

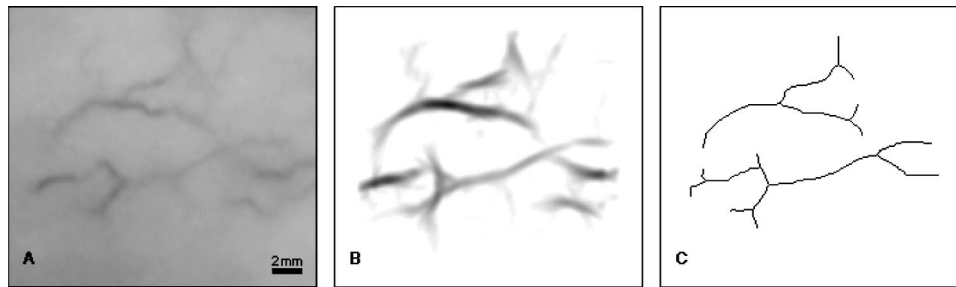


Fig. 6 Vessel detection: An example containing a few major vessels. (a) Original image. (b) Enhanced vessel image. (c) Vessel trace after segmentation.

Optics, E32-299). The beam diameter and focal length are chosen such that the beam NA nearly matches the acceptance NA of the fiber, while the size of the laser spot underfills the diameter of the fiber. The 4 m length of the fiber sufficiently mixes the light such that at the exit of the fiber both the size and the NA of the emitted light fill the fiber diameter and NA. A 650 nm diode laser (AIM, Coherent, 0221-899-50) is folded into the path via a dichroic mirror (M2). This aiming beam is also coupled into of the fiber via lens L1. The output power of the aiming beam is controlled by an analog output card (AO, National Instruments, PCI-6711) via the PC's PCI bus.

The light exiting the fiber face at the distal end of the fiber is imaged into the tissue plane with a $+6\times$ magnification using achromatic doublets L3 (Edmund Industrial Optics, E32-299) and L4 (Edmund Industrial Optics, E45-140) with focal lengths 12.5 and 75 mm, respectively. This results in a well-defined $300\ \mu\text{m}$ treatment beam spot size at the tissue plane. Lens L3 collimates the light emitted by the fiber into a 3 mm diameter beam, which is then reflected off of a pair of orthogonal galvometric scanners (G1 and G2, Cambridge Technologies, 6210). The galvometric scanners are each matched to a single-axis driver (Cambridge Technologies, MicroMax). This combination has a small step settling time of $120\ \mu\text{s}$, and allows the use of analog voltage for scan angle control, as well as analog positional feedback. The control voltage for the galvometric scanners is also supplied by the analog output card. The galvometric scanner position is read back with through the miscellaneous IO card. The galvometric scanners are placed near the front focal length of lens L4 to create a near-telecentric scan condition. At this location, an angular deflection of the galvometric scanner mirrors of $\pm 4.5^\circ$ is sufficient for full scan coverage of the beam over the $20\times 20\ \text{mm}$ area at the tissue. Lens L4 also

focuses the beam into the tissue plane. Furthermore, because of the small angles used in conjunction with the relatively long focal length of L4, $f \tan \theta \approx f\theta$, no correction is required to linearize the scanning. A full reflecting flat mirror (M3, Edmund Industrial Optics, E32-513) and a dichroic flat beam splitter (BS1, Absolute Coating, Custom) are placed in the path between L4 and the image plane in order to fold the beam into the camera's field of view. The beam splitter is coated such that it is a high reflector at 532 nm, a partial reflector at 650 nm, and transmits $\geq 80\%$ between 570 and 600 nm when placed at an angle of 55° . The thickness of this optic has been minimized to reduce astigmatism in the imaging system.

3 Principle of Operation

Light from both the 586 nm LED and the 650 nm aiming beam is efficiently imaged into the CCD. This is due to the multifunctional spectral characteristics of beam splitter, BS1. The vessel detection algorithm is applied to the LED illuminated images, providing a voltage map for the laser scanner galvonometers. The aiming beam illuminated images are used to verify the results of the algorithm. The scan starts at the endpoint that is closest to the upper-left-hand corner and follows that vessel to its conclusion. At branch points, the segment that requires the least change in scan direction is followed.

The beam can be swept over tissue at variable speeds. User input dictates the beam's dwell time on tissue, τ_d , by their choice of the expected vessel size range. Once this range of vessel sizes is chosen, a geometric mean is calculated to yield the value, d_v . The beam then moves such that a point on the tissue would be irradiated for at most $\tau_d = d_v^2 / 16\alpha$, where α is

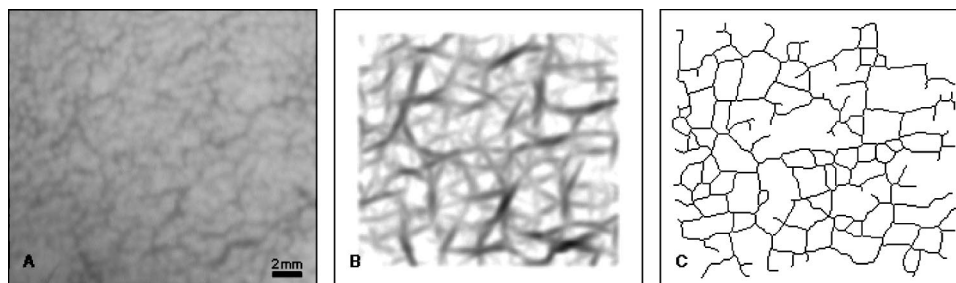


Fig. 7 Vessel detection: An example containing a large density of vessels of varying sizes. (a) Original image. (b) Enhanced vessel image. (c) Vessel trace after segmentation.

the thermal diffusivity of both blood and tissue, here considered to be the same as that of water, $\alpha=0.14\text{ mm}^2\text{ s}^{-1}$. Of course, this relation is only approximate. Note also that the dwell time is only accurate along the beam's center with respect to the scan direction. Obviously, the further towards the edges of the circular spot, the shorter the irradiation time. A $300\text{ }\mu\text{m}$ treatment beam spot size is chosen in order to have more uniform irradiance across the majority of clinically relevant vessels (diameter $\leq 200\text{ }\mu\text{m}$), while not overly compromising adjacent tissue. This also allows for some motion of the skin relative to the treatment beam, as might occur when deciding on scan direction between frames. Of course, a higher frame rate would obviate the need for any such over-compensation, and allow for smaller spots to be used when appropriate.

The current image processing algorithm, while optimized for this application, is still fairly computationally intensive and is the overall bandwidth bottleneck. The skeletonized image is updated approximately every 100 ms. The system then continues to scan along the line that most closely matches that of its last known location in the last frame. Because there is not a lot of movement normally possible in such a relatively short time span, this decision is made by simply comparing the pixels around the current scan location to those of the last frame. The respective vessel segment's directions are also compared in order to disallow any unexpected abrupt changes. This way a best match is easily made, and scanning is even and continuous. Vessels can be scanned any number of times, from only a single pass to continued scanning with the endpoint determined when the vessel can no longer be detected.

4 Conclusion

We have built a relatively small and inexpensive proof-of-principle system that is able to automatically detect and treat common telangiectasia in near real-time. However, we have not yet deployed the system clinically. Although the system is fully functional, there are a few upgrades that would go a long way to enhancing a next-generation device without further complicating the overall scheme. For instance, simply upgrading to a 2 GHz Pentium 4 machine, or switching to a distributed real-time operating system approach, would speed things up considerably and increase the margin of safety. Likewise, a digital camera would allow for greater flexibility in both imaging and illumination, especially when combined with a higher bit depth image acquisition board. With these improvements in computational depth and speed, more can be expected of the system. For example, the vessel width could be determined on the fly, and the scanning speed adjusted accordingly. Furthermore, once the vessel widths are known the scanning scheme could be tailored to the vessel type (vein versus artery) if there existed a mechanism to discriminate them. This could be done, for instance, by using a two-color illumination scheme that exploits the spectroscopic differences between oxy- and deoxy-hemoglobin. Vessels may then be scanned from their small segments towards their larger segments, or *vice versa* as appropriate for the type of vessel being treated. Future enhancements could also include spectral cube techniques for imaging and a servo zoom delivery

system to better match beam size to vessel size. Both of these, however, come at the expense of increasing system cost and complexity.

Acknowledgments

We would like to thank Stephen Pehrson for laying this project's groundwork while at Coherent Medical Group in 1995. Unfortunately, due to corporate restructuring, it laid dormant for quite some time. Therefore, we would also like to thank Dr. R. Rox Anderson of The Wellman Laboratories of Photomedicine at Massachusetts General Hospital for breathing new life into it.

References

1. E. F. Bernstein, "Treatment of a resistant port-wine stain with the 1.5-msec pulse duration, tunable, pulsed dye laser," *Dermatol. Surg.* **26**(11), 1007–1009 (2000).
2. J. Dover, "New approaches to the laser treatment of vascular lesions," *Australas. J. Dermatol.* **41**(1), 14–18 (2000).
3. K. Arndt, "Argon laser therapy of small cutaneous vascular lesions," *Arch. Dermatol.* **118**, 220–224 (1982).
4. Adrianna Scheibner and Ronald Wheeland, "Argon-pumped tunable dye laser therapy for facial port-wine stain hemangiomas in adults—a new technique using small spot size and minimal power," *J. Dermatol. Surg. Oncol.* **15**(3), 277–282 (1989).
5. R. R. Anderson (personal communication).
6. E. L. Sebern, C. J. H. Brenan, R. R. Anderson, and I. W. Hunter, "Tissue modification with feedback: the 'smart scalpel,'" *Proc. SPIE* **3519**, 62–69 (1998).
7. E. L. Sebern, C. J. H. Brenan, R. R. Anderson, and I. W. Hunter, "Laser treatment of nevus flammeus (port wine stain) with spectroscopic feedback: the 'smart scalpel,'" *Proc. SPIE* **3590**, 32–42 (1999).
8. E. L. Sebern, C. J. H. Brenan, and I. W. Hunter, "Design and characterization of a laser-based instrument with spectroscopic feedback control for treatment of vascular lesions: the 'smart scalpel,'" *J. Biomed. Opt.* **5**(4), 375–382 (2000).
9. K. H. Lim, C. J. H. Brenan, R. R. Anderson, and I. W. Hunter, "Microsurgical laser scalpel based on spectroscopic feedback: The 'smart scalpel,'" *Proc. SPIE* **4244**, 25–35 (2001).
10. G. M. J. Bos, D. W. Slaaf, G. D. Majoor, G. J. Tangelder, and R. S. Reneman, "A model for chronic study vascular morphology and reactivity of physically intact rat skin microcirculation," *Int. J. Microcirc.: Clin. Exp.* **6**, 371–380 (1987).
11. J. Philip, N. J. Carter, and C. P. Lenn, "Improved optical discrimination of skin with polarized light," *J. Soc. Cosmet. Chem.* **39**, 121–132 (1988).
12. S. Chaudhuri, S. Chatterjee, N. Katz, and M. Goldbaum, "Detection of blood vessels in retinal images using two-dimensional matched filters," *IEEE Trans. Med. Imaging* **8**(3), 263–269 (1989).
13. Riccardo Poli and Guido Valli, "An algorithm for real time vessel enhancement and detection," *Comput. Methods Programs Biomed.* **52**(1), 1–22 (1997).
14. B. L. Côté, W. E. Hart, M. H. Goldbaum, P. Kube, and M. Nelson, "Classification of blood vessels in images of the ocular fundus," Technical Report CS94-350, University of California, San Diego, 1994.
15. J. Canny, "Finding edges and lines in images," Technical Report 720, MIT Artificial Intelligence Laboratory, 1983.
16. J. Canny, "A computational approach to edge detection," *IEEE Trans. Pattern Anal. Mach. Intell.* **PAMI-8**(6), 679–697 (1986).
17. R. J. Elble and W. C. Koller, *Tremor*. The Johns Hopkins University Press, Baltimore (1990).
18. M. A. Niczyporuk, D. E. Andersen, M. W. Wiltberger, and D. G. Angeley, "An algorithm for the near real time detection and tracking of telangiectatic vessels in human skin," to be published.
19. M. Nelson, N. Katz, M. Goldbaum, and S. Chaudhuri, "An image processing system for automatic retinal diagnosis," *Proc. SPIE* **902**, 131–137 (1988).
20. M. A. Fischler, "Detection of roads and linear structures in low reso-

- lution aerial imagery using a multisource knowledge integration technique,” *Comput. Graph. Image Process.* **15**(3), 201–223 (1981).
21. F. W. M. Stentiford, “Some new heuristics for thinning binary hand-printed characters for OCR,” *IEEE Trans. Syst. Man Cybern.* **13**(1), 81–84 (1983).
 22. T. Y. Zhang and C. Y. Suen, “Fast parallel thinning for digital patterns,” *Commun. ACM* **27**(3), 236–239 (1984).
 23. Christopher M. Holt, Alan Stewart, Maurice Clint, and Ronald H. Perrott, “Improved parallel thinning algorithm,” *Commun. ACM* **30**(2), 156–160 (1987).